Dalton Transactions

Accepted Manuscript

ROYAL SOCIETY OF CHEMISTRY

www.rsc.org/dalton

Ternary rare earth silicides $RE_2M_3Si_4$ (RE = Sc, Y, Lu; M = Mo, W): crystal structure, coloring and electronic properties

Morten B. Nielsen,[1,2] Weiwei Xie[2] and Robert J. Cava[2]

[1]Center for Materials Crystallography, Department of Chemistry, Aarhus University, 8000 Aarhus C, Denmark

[2]Department of Chemistry, Princeton University, Princeton, 08540 NJ, USA

Abstract

The ternary compounds $Sc_2Mo_3Si_4$, $Y_2Mo_3Si_4$, $Lu_2Mo_3Si_4$ and $Sc_2W_3Si_4$ have been synthesized using arc melting and structurally characterized using single crystal x-ray diffraction. The compounds are isostructural with Gd_5Si_4 but with coloring (order of the rare earth and transition metals) on the Gd site. In contrast to group 4 and 5 ternaries of the same type, we observe no site mixing between the rare earth and transition metals. The Y compound displays a different, less common coloring from the others and through DFT calculations and investigation of the solid solution between $Sc_2Mo_3Si_4$ and $Y_2Mo_3Si_4$ it is shown that the different coloring of the latter is only marginally more stable. The electronic structures of the ternary compounds have been investigated using DFT calculations, yielding densities of states very similar to Gd_5Si_4. These predict metallic behavior and no magnetism, which is confirmed through resistivity and magnetization measurements.

Key words: Gd_5Si_4 structure, solid solution, rare earth intermetallics, coloring

1. Introduction

Rare earth tetrelides (Tt) of the stoichiometry RE_5Tt_4 (Tt = Si or Ge) have attracted considerable attention for application in solid-state magnetic refrigeration.[1, 2] Optimal materials for this application display magnetic and structural phase transitions with large entropy changes that are close to each other in temperature. In addition to their rich, subtle and complex structural chemistry, the compounds also host giant magnetoresistance and other interesting magnetic behaviors such as magnetostriction or magnetic glass states.[3] A well written tutorial review by Miller[4] provides a good introduction to this interesting field.

The central motif often employed to explain these structures is a $RETt_6$ octahedron resting inside a RE_8 pseudo-cube, as shown in Fig. 1 left. In the case of Gd_5Si_4 the cube is connected to a neighboring cube through a Tt-Tt bond, while other compounds such as Sm_5Ge_4 do not feature this bond. The cubes link together through edge sharing to form an infinite slab in a pattern that features another Tt-Tt bond, where each Tt atom is in a trigonal prismatic coordination.

Within this class of materials, considerable attention has been paid to isovalent substitution of both anions on the tetrelide site[5-14] and rare earths on the cation site.[15-18] Both kinds of tuning induce subtle changes in the tetrelide bonding within the structures, and also affect the magnetic

interactions. As a result, substantial changes in the magnetic ordering and structural transition temperatures can be obtained. The problem of determining the degree of site mixing (or order) in the cation lattice is known as the coloring problem.[19]

Another well-explored avenue of research in the field involves manipulation of the valence electron count (VEC) of the compounds in order to investigate the effect this has on the Tt-Tt bonding. Introducing lower valence cations (usually group 2) lowers the VEC in the compounds, and it has been demonstrated that this leads to Tt-Tt bond formation by reducing the occupation of antibonding Tt states.[20, 21] This in turn has implications for both magnetic and structural transition temperatures.

Increasing the VEC by substitution of group 4 and 5 transition metals for the rare earths has also been explored. This increases the VEC and one might expect the result to be opposite of the lower valence doping, namely a marked weakening of the Tt-Tt bonds. However, owing to the higher electronegativity of transition metals from group 4 and 5 compared to the rare earths and group 2 elements, the charge transfer from the metals to the Tt network appears to be much smaller.[22] As a result, the relationship between VEC and Tt-Tt bond lengths are complicated by the presence of covalency, the degree of which also depends on the tetrelide. For instance, the Tt-Tt bond lengths are only affected to a small degree by the VEC changes in $Gd_{5-x}Zr_xSi_4$,[23] while the increase in VEC drastically strengthens the bond in the case of $Gd_{5-x}Zr_xGe_4$.[24]

Another equally important effect of the higher electronegativity on the metal lattice is on the coloring. Generally speaking, cations with higher electronegativities prefer lower coordination numbers,[19] which in turn leads to (partial) site order when the transition metal is introduced. The element specific site preference increases (they become more ordered) when going from group 4 to group 5, with roughly 16 % site mixing in $Gd_{1.94}Zr_{3.06}Si_4$ and 6 % in $Sc_{2.04}Nb_{2.96}Ge_4$.[22, 23]

In this paper we expand the range of explored mixed rare earth transition metal tetrelides to group 6, by the structural and property characterization of $Sc_2Mo_3Si_4$, $Y_2Mo_3Si_4$, $Lu_2Mo_3Si_4$ and $Sc_2W_3Si_4$. Of these, $Lu_2Mo_3Si_4$ has not been reported before, atomic coordinates have been reported for $Y_2Mo_3Si_4$ based on single crystal x-ray diffraction,[25] and $Sc_2Mo_3Si_4$ and $Sc_2W_3Si_4$ have only had their powder patterns indexed and unit cell dimensions reported.[26-28] The physical properties of all but $Y_2Mo_3Si_4$ are to our knowledge hitherto unexplored.

2. Methods

Polycrystalline samples were synthesized by arc-melting elemental precursors under an argon atmosphere on a water-cooled copper hearth. Si (99.9999 %, Alfa Æsar), and the rare earths (99.9 %, Alfa Æsar) came in the form of chunks while powders of Mo (99.9 %, Alfa Products), Nb (99.9 %, Æsar) and W (99.9 %, Alfa Products) were compressed into pellets before melting. Rare earths were weighed out in an Ar filled glove box and subsequently transferred to the arc-welder located outside the glove box. The oxide contamination observed in the powders arose from air exposure during transfer and pellet stacking. Each sample was turned over and re-melted at least twice to ensure good mixing. The total mass loss after each synthesis was typically about 1 %.

Single crystal x-ray diffraction was measured on crystals extracted from the arc-melted samples. The measurements were carried out on a Bruker APEX II diffractometer with Mo K_α radiation while the structure was solved using direct methods and refined by full-matrix least squares on F^2 with the SHELXT package.[29, 30] Further details of the crystal structure investigations may be obtained from FIZ Karlsruhe, 76344 Eggenstein-Leopoldshafen, Germany (fax: (+49)7247-808-666; e-mail: crysdata@fiz-karlsruhe.de, on quoting the deposition numbers CSD-430055 ($Sc_2Mo_3Si_4$), CSD-430105 ($Sc_2W_3Si_4$) and CSD-430056 ($Lu_2Mo_3Si_4$).

Powder x-ray diffraction (PXRD) was collected on powders of the crushed and ground samples, using Ni-filtered Cu K_α radiation on a Bruker D8 Advance ECO diffractometer with a LynxEye-XE detector. The resulting powder patterns were modeled using the MAUD program[31] and impurity phases were modeled where present. All crystal structure drawings were produced using the program VESTA.[32]

Magnetization measurements were performed on a Quantum Design, Inc., superconducting quantum interference device (SQUID) magnetometer, using an applied field of 10 Oe at 1.8 K. Resistivity versus temperature was measured using a Quantum Design Physical Property Measurement System (PPMS) from 300 to 2 K.

The electronic structure calculations were performed by density functional theory (DFT) using the WIEN2K code with a full-potential linearized augmented plane-wave and local orbitals (FP-LAPW + lo) basis[33] together with the PBE parameterization[34] of the GGA, including spin orbit coupling (SOC). The plane-wave cutoff parameter $R_{MT}K_{MAX}$ was set to 7 and the Brillouin zone was sampled by 1000 k points. Convergence was confirmed by increasing $R_{MT}K_{MAX}$ until no change in total energy or charge was observed.

3. Results and discussion

3.1 $Sc_2Mo_3Si_4$ crystal structure

The structure of $Sc_2Mo_3Si_4$ as obtained from single crystal x-ray diffraction (SC-XRD) can be seen in Fig. 1 middle, with the crystallographic details supplied in Table 1 and 2. This structure has previously been indexed by Kotur et al.[26] who claimed that it fit the $Ce_2Sc_3Si_4$ structure type, which we here confirm. Our lattice parameter results are in good agreement with those reported previously, though the values in the ICSD entry for the compound (no. 644333) differ from those found in references.[26, 27] No atomic positions have been reported before, but the obtained relative coordinates closely match those of Gd_5Si_4. A CIF of the structure is given in the Electronic Supplementary Information (ESI).

The overall structural motif of $Sc_2Mo_3Si_4$ is the same as in Gd_5Si_4, with the added complexity that the Sc atoms all occupy one face of the pseudo-cube, with the Mo on the other face. The $MoSi_6$ octahedra link through a 2.488(2) Å Si-Si bond along the *b*-axis of the structure, while the in-slab Si-Si bond length is 2.497(2) Å. On the metal lattice, we do not observe any site mixing of Sc and Mo. This is interesting as quite significant site mixing is observed in $Gd_{1.94}Zr_{3.06}Si_4$ (henceforth referred to as $Gd_2Zr_3Si_4$) on all three metal sites.[23] This difference can be understood by combining the mentioned tendency for more electronegative cations to prefer lower

coordination numbers[19] with the observation that Mo has a much higher electronegativity (χ = 2.16) than Zr (χ = 1.33), while Sc (χ = 1.36) has about the same as Gd (χ = 1.20).[35] The electronegativity contrast, and thus site preference, between the two metals is thus much greater than in $Gd_2Zr_3Si_4$ leading to no detectible site mixing. The result is that all Mo are coordinated by six Si atoms, while all Sc are coordinated by seven Si atoms. The Mo-Si bond lengths lie between 2.543(2) and 2.733(2) Å in the regular octahedron (Mo2) and between 2.483(1) and 2.569(1) Å in the distorted one (Mo1), indicating that the distorted coordination environment leads to stronger bonding.

It should be noted that in some previous reports on $Sc_2Mo_3Si_4$ this structure is referred to as an ordered superstructure of the Sm_5Ge_4 structure type, while it is technically a cation ordered version of the Gd_5Si_4 type. The two structures are isopointal (that is, both are *Pnma*), but have substantially different bonding arrangements, distinguished by the presence of the Tt-Tt bond linking the octahedron inside the RE_8 pseudo-cubes in Gd_5Si_4 (in our case the cubes are Sc_4Mo_4) that is not present in Sm_5Ge_4.

3.2 $Sc_2W_3Si_4$ crystal structure

SC-XRD data on $Sc_2W_3Si_4$ shows that substituting W for Mo does not result in a change of structure, and only very slightly expands the volume of the unit cell in agreement with previous indexing of this compound.[28] The crystallographic details are supplied in Table 1 and 2, while a CIF of the structure is given in the ESI. The atomic coordinates are again very close to those found in Gd_5Si_4. The single crystal refinement shows that the stoichiometry is slightly off from the nominal composition, being $Sc_{2.066(4)}W_{2.934(4)}Si_4$. The excess Sc is located on the W pseudo-cube site, while no Sc could be detected at the octahedral site. This can be rationalized in terms of considering that a W^{3+} $5d^3$ ion displays an (admittedly small) octahedral stabilization while Sc^{3+} does not and thus the energy penalty of placing Sc in the octahedral site would be higher.

The bonding in the W variant shows an inter-cube Si-Si bond length of 2.508(2) Å and an in-slab Si-Si distance of 2.487(3) Å. The W-Si bond lengths in the octahedron (W2) fall between 2.545(2) and 2.740(3) Å, while the distorted coordination (W1) shows lengths between 2.493(1) and 2.603(2) Å. As in $Sc_2Mo_3Si_4$, this difference in bond lengths indicates stronger metal to silicon interactions on the irregular site.

3.3 $Y_2Mo_3Si_4$ crystal structure

Progressing down group 3 to Y results in a different, but similar structure for $Y_2Mo_3Si_4$. This structure was solved by SC-XRD by Bodak et al.,[25] who found that it crystallizes in the $U_2Mo_3Si_4$ structure type. Fig. 1 right illustrates how it relates to $Sc_2Mo_3Si_4$, in that the overall motif is the same, but Y is separated into two pairs on opposite sides of the cube of atoms surrounding the $MoSi_6$ octahedron. The result of a full Rietveld refinement of the $Y_2Mo_3Si_4$ structure on our PXRD data resulted in lattice parameters that agree to within 0.1% of the single crystal results of Bodak et al. The data and refinement are given in the ESI.

The inter-cube Si-Si bond is also present in $Y_2Mo_3Si_4$, being 2.536 Å while the in-slab Si-Si bond is 2.470 Å. The Mo-Si bonds follow the same pattern as in $Sc_2Mo_3Si_4$, giving lengths of

2.680 to 2.691 Å for the regular octahedron and 2.541 to 2.634 Å for the distorted one (all calculated from the structure reported by Bodak et al.). These bonds are thus longer than in the Sc variant and the distribution of bond lengths is narrower. Without going into detailed calculations of the crystal orbitals, we speculate that the slightly lower electronegativity of Y (χ = 1.22) compared to Sc (χ = 1.36) results in a slightly increased amount of electron donation to the lattice, where they populate antibonding Mo-Si states.

3.4 $(Sc,Y)_2Mo_3Si_4$ solid solution

A solid solution is formed between $Sc_2Mo_3Si_4$ and $Y_2Mo_3Si_4$. The evolution of volume per formula unit of the solid solution is shown in Fig. 2. The first axis of the plot is the averaged rare earth atomic radius. The solid solution follows Vegard's law well, in spite of the change in coloring of the cation lattice at high Y content. That the change in structure type occurs relatively close to the Y end member could suggest that the arrangement of the rare earth atoms on opposite sides of the RE_4Mo_4 cube is only marginally more stable than the clustered arrangement. DFT total energy calculations on $Y_2Mo_3Si_4$ in the two structures supports this view as it shows the $U_2Mo_3Si_4$ type to be favored by 1.82 eV per formula unit, a small but non-trivial energy difference. The nearest shell Si coordination of the rare earth ion is essentially identical in both structures and so the energy difference must stem from the second shell cation coordination where the presence of a RE-RE contact that is swapped for a RE-Mo contact in the $U_2Mo_3Si_4$ variant. It thus seems like a narrow set of conditions have to be fulfilled to stabilize the $U_2Mo_3Si_4$ type coloring over the $Ce_2Sc_3Si_4$ coloring, explaining why the former is much less common.

3.5 $Lu_2Mo_3Si_4$ crystal structure

When the intermediary sized Lu is used as the rare earth it is also possible to create a compound with the same stoichiometric ratio, $Lu_2Mo_3Si_4$. This compound, which to our knowledge has not been reported previously, was solved using SC-XRD and is isostructural with $Sc_2Mo_3Si_4$. The crystallographic details are given in Tables 1 and 2, with the relative atomic positions also here being very similar to the parent Gd_5Si_4. The inter-cube bond is 2.506(3) Å while the in-slab dimer bond length is 2.538(4) Å. The Mo-Si bonds are all slightly longer than in the Sc variant but show the same trend, with the distances in the regular octahedron (Mo2) being longer at 2.611(3) to 2.713(3) Å compared to the distorted one (Mo1) which falls between 2.512(2) and 2.622(2) Å. A CIF of the structure is given in the ESI.

That the Lu variant appears in this structure is consistent with the trend of the Sc-Y solid solution series, where the size of Lu[35] places it near the (25/75% Sc/Y) volume per formula unit (see Fig. 2). Like the Sc variant we observe no site mixing between Lu and Mo. Invoking the same reasoning as for $Sc_2Mo_3Si_4$, the Lu variant is even less likely to feature mixing as the electronegativity of Lu (χ = 1.27) is lower than that of Sc.

3.6 Electronic structure calculations

The electronic band structure of $Sc_2Mo_3Si_4$ near the Fermi level and its density of states (DOS) are shown in Fig. 3a, while the corresponding electronic band structure of $Lu_2Mo_3Si_4$ is shown in Fig. 3b along with its DOS. An expanded energy range total DOS plot is given for each in Fig. 4.

In both compounds the Fermi level rests in a narrow pseudo-gap in the DOS. This contrasts the total DOS of the parent compound Gd_5Si_4 where the DOS at the Fermi level is fairly large.[36] In Gd_5Si_4, Gd *d* states dominate the total DOS at the Fermi level, while in our mixed cation case both Sc and Lu as well as the Mo valence orbitals contribute much less to the DOS at this energy. Both compounds display another wider pseudo-gap about 0.6 eV below the Fermi level, at an electron count of 38 (two below the full valence electron count 40). A similar pseudo-gap is also found in Gd_5Si_4 and the isostructural low temperature/high magnetic field FM O(I) modification of Gd_5Ge_4.[36, 37] Aside from a few small electron and hole pockets the Fermi level cuts through highly dispersive bands in the Sc variant. A couple of the pockets are eliminated in the Lu variant, lowering the total DOS at the Fermi level, but otherwise the overall topology is the same, with a few shifts of bands that are heavy in Lu contribution.

The electronic band structure of $Y_2Mo_3Si_4$ near the Fermi level can be seen in Fig. 5 along with its DOS. An expanded energy range total DOS for this compound is also given in Fig. 4. Like the two previous compounds, the Fermi level is located at a pseudo-gap, with the total DOS being about the same as that of $Lu_2Mo_3Si_4$. In spite of the lower symmetry and different coloring, it displays an electronic band structure whose total DOS is very similar to $Sc_2Mo_3Si_4$ and $Lu_2Mo_3Si_4$, including the Gd_5Si_4 pseudo-gap slightly below the Fermi level. Aside from one band between Γ and Z which displays an interesting crossing below the Fermi level, the states all belong to either electron or hole pockets.

The calculations for all three compounds thus indicate that they have low densities of electronic states near the Fermi level at their stoichiometric compositions. Features that might hint at either magnetic order or superconductivity, such as DOS peaks or van Hove singularities at or near the Fermi level, are absent.

3.7 Electronic transport properties and magnetism

Resistivity as a function of temperature for the Sc, Y and Lu combinations with Mo and Si are shown in Fig. 6. Since the arc melted pellets are not phase pure (see PXRD in the ESI) and the significant impurities are all metallic (ρ_{300K} on the order of 20 to 100 μΩ cm) the measurements should be considered a lower bound of the true value as we measure much higher resistivities (ρ_{300K} > 0.4 mΩ cm for all samples). The $Sc_2W_3Si_4$ pellet showed a resistivity that was basically identical to the main impurity WSi_2 and is thus not included. From the residual resistivity ratios it is also clear that these compounds should be classified as bad metals, with ratios spanning between 1.28 for $Lu_2Mo_3Si_4$ and 2.63 for $Y_2Mo_3Si_4$. SQUID measurements yield weak paramagnetic signals at 1.8K for all the samples, indicating that no magnetic order or superconductivity is present down to this temperature. All of the above is in good agreement with the calculated electronic structures of the compounds.

4. Conclusion

The mixed rare earth transition metal tetrelides $Sc_2Mo_3Si_4$, $Y_2Mo_3Si_4$, $Lu_2Mo_3Si_4$ and $Sc_2W_3Si_4$ have been synthesized using arc melting and their crystal structures investigated using single crystal x-ray diffraction. All of the compounds crystallize in so called colored versions of the Gd_5Si_4 structure, with the ordering scheme of the Y variant different from the three other

compounds. The coloring schemes and variations Tm-Si bond lengths across the series have been rationalized in terms of the differences in electronegativity between the rare earth and transition metals employed. The $Sc_2Mo_3Si_4$ structure type is stable over the majority of the solid solution between $Sc_2Mo_3Si_4$ and $Y_2Mo_3Si_4$, with DFT showing the latter coloring to be only marginally more stable than the $Sc_2Mo_3Si_4$ coloring scheme for this element.

The band structures of the compounds have been calculated using DFT and show that placing the Fermi level in a pseudo-gap in the electronic band structure stabilizes all of them. The total DOS of the compounds are very similar to the total DOS of Gd_5Si_4, with another pseudo-gap located about 0.6 eV below the Fermi level, at an electron count of 38 (two below the full count of 40). Resistivity and magnetization measurements on the three first compounds show that they are all bad metals that display no magnetic order or superconductivity down to 2 K.

Acknowledgements

MBN wishes to thank Quinn D. Gibson for help with the DFT calculations, and Quinn D. Gibson and Elizabeth M. Seibel for helpful discussions. MBN gratefully acknowledges the Danish Ministry of Higher Education and Science for a travel scholarship supporting his stay at Princeton University. The work at Princeton University, which included materials synthesis, electronic structure calculations, and diffraction and property characterization, was supported by the US Department of Energy Division of Basic Energy Sciences, grant DE-FG02-98ER45706.

Notes and References

Electronic Supplementary Information (ESI) available: Crystallographic Information Files (CIFs) of $Sc_2Mo_3Si_4$, $Sc_{2.07}W_{2.93}Si_4$ and $Lu_2Mo_3Si_4$, Rietveld refinement obs.-calc. diagrams for the different samples (Fig. S1-4). See DOI: 10.1039/b000000x/

1. K. A. Gschneidner, V. K. Pecharsky and A. O. Tsokol, *Rep. Prog. Phys.*, 2005, **68**, 1479-1539.
2. K. A. Gschneidner and V. K. Pecharsky, *Int. J. Refrig.*, 2008, **31**, 945-961.
3. Y. Mudryk, V. K. Pecharsky and K. A. Gschneidner, *Z. Anorg. Allg. Chem.*, 2011, **637**, 1948-1956.
4. G. J. Miller, *Chem. Soc. Rev.*, 2006, **35**, 799-813.
5. V. K. Pecharsky and K. A. Gschneidner, *Adv. Cryog. Eng.*, 1998, **43**, 1729-1736.
6. C. Ritter, L. Morellon, P. A. Algarabel, C. Magen and M. R. Ibarra, *Phys. Rev. B: Condens. Matter Mater. Phys.*, 2002, **65**.
7. Y. Mozharivskyj, W. Choe, A. O. Pecharsky and G. J. Miller, *J. Am. Chem. Soc.*, 2003, **125**, 15183-15190.
8. A. O. Pecharsky, K. A. Gschneidner, V. K. Pecharsky, D. L. Schlagel and T. A. Lograsso, *Phys. Rev. B: Condens. Matter Mater. Phys.*, 2004, **70**.
9. A. O. Pecharsky, V. K. Pecharsky and K. A. Gschneidner, *J. Alloys Compd.*, 2004, **379**, 127-134.
10. K. Ahn, A. O. Tsokol, Y. Mozharivskyj, K. A. Gschneidner and V. K. Pecharsky, *Phys. Rev. B: Condens. Matter Mater. Phys.*, 2005, **72**.
11. Y. Mozharivskyj, A. O. Tsokol and G. J. Miller, *Z. Kristallogr.*, 2006, **221**, 493-501.
12. K. Ahn, V. K. Pecharsky and K. A. Gschneidner, *Phys. Rev. B: Condens. Matter Mater. Phys.*, 2007, **76**.
13. A. Y. Kozlov, V. V. Pavlyuk and V. M. Davydov, *Intermetallics*, 2004, **12**, 151-155.
14. A. Guloy and J. D. Corbett, *J. Solid State Chem.*, 2005, **178**, 1112-1124.

15. U. C. Rodewald, B. Heying, D. Johrendt, R. D. Hoffmann and R. Pottgen, *Z. Naturforsch., B: J. Chem. Sci.*, 2004, **59**, 174-181.
16. H. Wang, F. Wang, K. Jones and G. J. Miller, *Inorg. Chem.*, 2011, **50**, 12714-12723.
17. J. L. Yao, P. L. Wang and Y. Mozharivskyj, *J. Alloys Compd.*, 2012, **534**, 74-80.
18. Y. Mudryk, V. K. Pecharsky and K. A. Gschneidner, *J. Appl. Phys. (Melville, NY, U.S.)*, 2013, **113**.
19. G. J. Miller, *Eur. J. Inorg. Chem.*, 1998, 523-536.
20. L. M. Wu, S. H. Kim and D. K. Seo, *J. Am. Chem. Soc.*, 2005, **127**, 15682-15683.
21. P. H. Tobash, S. Bobev, J. D. Thompson and J. L. Sarrao, *Inorg. Chem.*, 2009, **48**, 6641-6651.
22. B. Reker, S. F. Matar, U. C. Rodewald, R. D. Hoffmann and R. Pottgen, *Z. Naturforsch., B: J. Chem. Sci.*, 2013, **68**, 625-634.
23. J. L. Yao, P. Lyutyy and Y. Mozharivskyj, *Dalton Trans.*, 2011, **40**, 4275-4283.
24. J. L. Yao and Y. Mozharivskyj, *Z. Anorg. Allg. Chem.*, 2011, **637**, 2039-2045.
25. O. I. Bodak, Y. K. Gorelenko, V. I. Yarovets and R. V. Skolozdra, *Inorg. Mater.*, 1984, **20**, 741-743.
26. B. Y. Kotur, O. I. Bodak and V. E. Zavodnik, *Kristallografiya*, 1986, **31**, 868-873.
27. B. Y. Kotur and O. I. Bodak, *Russ. Metall. (Engl. Transl.)*, 1988, 193-196.
28. B. Y. Kotur, O. M. Boznyak and O. I. Bodak, *Inorg. Mater.*, 1989, **25**, 345-348.
29. J. Waser, *Acta Crystallogr.*, 1963, **16**, 1091-&.
30. G. M. Sheldrick, *Acta Crystallogr., Sect. A: Found. Crystallogr.*, 2008, **64**, 112-122.
31. L. Lutterotti, S. Matthies, H. R. Wenk, A. S. Schultz and J. W. Richardson, *J. Appl. Phys. (Melville, NY, U.S.)*, 1997, **81**, 594-600.
32. K. Momma and F. Izumi, *J. Appl. Crystallogr.*, 2011, **44**, 1272-1276.
33. P. Blaha, K. Schwarz, G. Madsen, D. Kvasnicka and J. Luitz, *WIEN2k*, An augmented Plane Wave + Local Orbitals Program for Calculating Crystal Properties (Karlheinz Schwarz, Techn. Universität Wien, Austria), 2001. ISBN 3-9501031-1-2.
34. J. P. Perdew, K. Burke and M. Ernzerhof, *Phys. Rev. Lett.*, 1996, **77**, 3865-3868.
35. R. D. Shannon, *Acta Crystallogr., Sect. A: Cryst. Phys. Diffr. Theor. Gen. Cryst.*, 1976, **32**, 751-767.
36. G. Skorek, J. Deniszczyk and J. Szade, *J. Phys.: Condens. Matter*, 2002, **14**, 7273.
37. E. M. Levin, V. K. Pecharsky, K. A. Gschneidner and G. J. Miller, *Phys. Rev. B: Condens. Matter Mater. Phys.*, 2001, **64**.

Table 1 – Crystallographic information for the structure refinements of $Sc_2Mo_3Si_4$, $Sc_2W_3Si_4$ and $Lu_2Mo_3Si_4$ crystals at room temperature using Mo K_α radiation on a Bruker APEX-II CCD diffractometer.

Sample	$Sc_2Mo_3Si_4$	$Sc_2W_3Si_4$	$Lu_2Mo_3Si_4$
Refined comp.	Stoichiometric within 0.01	$Sc_{2.066(4)}W_{2.934(4)}Si_4$	Stoichiometric within 0.01
Space group	*Pnma*	*Pnma*	*Pnma*
Lattice parameters (Å)	a = 6.5175(5) b = 12.6141(10) c = 6.7628(5)	a = 6.5357(4) b = 12.6408(8) c = 6.7743(4)	a = 6.6451(3) b = 12.7818(6) c = 6.8725(3)
Volume / f.u. ($Å^3$)	139.00(2)	139.92(2)	145.93(1)
θ range	3.230 to 29.965°	3.223 to 30.538°	3.188 to 29.584°
Data/parameters	823/47	897/48	853/46
GOF on F^2	1.172	1.138	0.999
R ($I > 2\sigma$)	R_1 = 0.0217 wR_2 = 0.0581	R_1 = 0.0232 wR_2 = 0.0380	R_1 = 0.0300 wR_2 = 0.0428
Peak/hole, e/$Å^3$	1.6/ -0.88	1.7/-1.9	1.4/-1.7

Table 2 – Atomic coordinates and thermal displacement parameters (U_{eq}) for $Sc_2Mo_3Si_4$ and $Lu_2Mo_3Si_4$ obtained by single crystal x-ray diffraction.

$Sc_2Mo_3Si_4$						
Atom	Site	Occupancy	*x*	*y*	*z*	U_{eq} (Å^2)
Sc1	8*d*	1	-0.00476(9)	0.59174(5)	0.17084(9)	0.0025(2)
Mo1	8*d*	1	0.32886(4)	0.12381(2)	0.16560(4)	0.0048(1)
Mo2	4*c*	1	0.16452(6)	¼	0.50552(6)	0.0042(1)
Si1	8*d*	1	0.16623(1)	0.04415(8)	0.4625(2)	0.0062(2)
Si2	4*c*	1	0.0314(2)	¼	0.1223(2)	0.0064(3)
Si3	4*c*	1	0.2997(2)	¼	0.8588(2)	0.0060(3)
$Sc_{2.066}W_{2.934}Si_4$						
Atom	Site	Occupancy	*x*	*y*	*z*	U_{eq} (Å^2)
Sc1	8*d*	1	-0.0045(2)	0.59149(7)	0.1707(1)	0.0022(2)
W1	8*d*	0.967(2)*	0.32973(3)	0.12423(2)	0.16485(3)	0.00086(8)
W2	4*c*	1	0.16335(4)	¼	0.50255(4)	0.00041(9)
Si1	8*d*	1	0.1677(2)	0.04373(12)	0.4623(2)	0.0016(3)
Si2	4*c*	1	0.0320(3)	¼	0.1185(3)	0.0016(4)
Si3	4*c*	1	0.2990(3)	¼	0.8570(3)	0.0015(4)
* Remainder of this site is Sc at an occupancy 1 – occ(W) = 0.033(2)						
$Lu_2Mo_3Si_4$						
Atom	Site	Occupancy	*x*	*y*	*z*	U_{eq} (Å^2)
Lu1	8*d*	1	-0.00258(4)	0.59325(2)	0.16871(3)	0.00466(8)
Mo1	8*d*	1	0.32977(8)	0.12404(4)	0.16668(6)	0.0038(1)
Mo2	4*c*	1	0.16575(11)	¼	0.50378(9)	0.0035(1)
Si1	8*d*	1	0.1616(3)	0.0457(1)	0.4599(2)	0.0048(3)
Si2	4*c*	1	0.0334(4)	¼	0.1303(3)	0.0055(5)
Si3	4*c*	1	0.3011(4)	¼	0.8669(3)	0.0050(5)

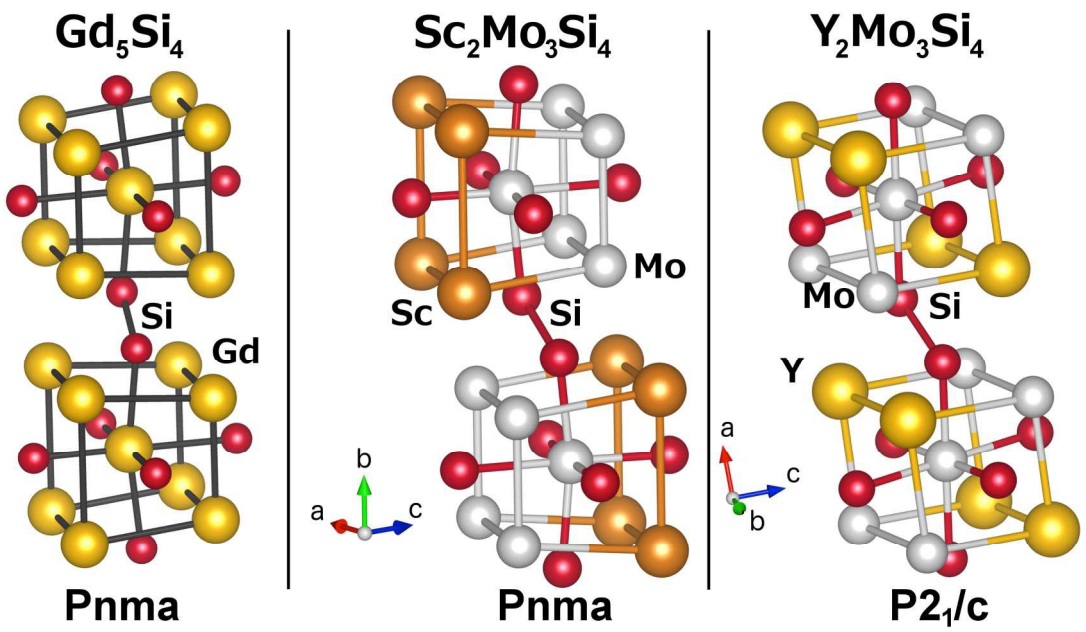

311

312 Figure 1. Left: The central pseudo-cube motif of Gd_5Si_4 with the Si-Si bond linking the cubes.
313 Center: The $Sc_2Mo_3Si_4$ structure. The rare-earth ions are all located on one side of the cube of
314 atoms surrounding the MSi_6 octahedron. Right: The $Y_2Mo_3Si_4$ structure. Here the rare-earth ions
315 sit in pars opposite each other on the cube.

316

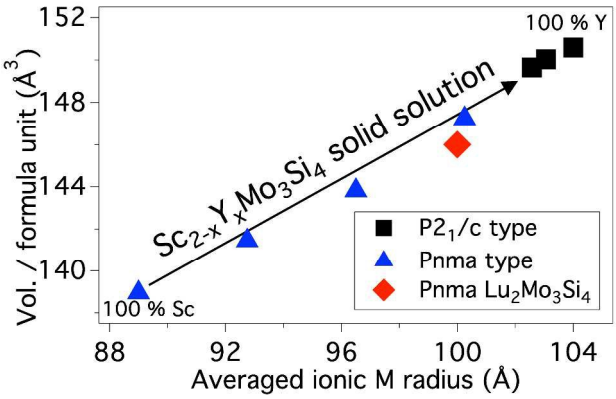

Figure 2. The volume per formula unit in the solid solution series $Sc_{2-x}Y_xMo_3Si_4$, with $0 < x < 2$. Blue triangles show samples that crystallized in the $Sc_2Mo_3Si_4$ type, while black squares show the samples that displayed the $Y_2Mo_3Si_4$ structure. The first axis shows the averaged ionic radius of the rare earth mixture, facilitating comparison with $Lu_2Mo_3Si_4$, which is isostructural with $Sc_2Mo_3Si_4$.

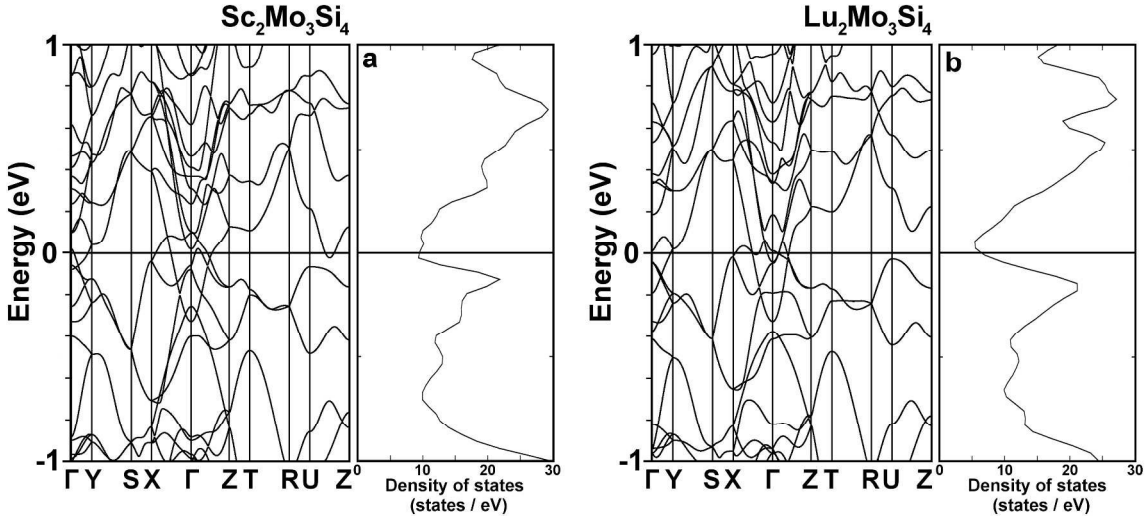

Figure 3. a) Electronic band structure of *Pnma*-symmetry $Sc_2Mo_3Si_4$ and total density of states. b) Electronic band structure of *Pnma*-symmetry $Lu_2Mo_3Si_4$ and total density of states.

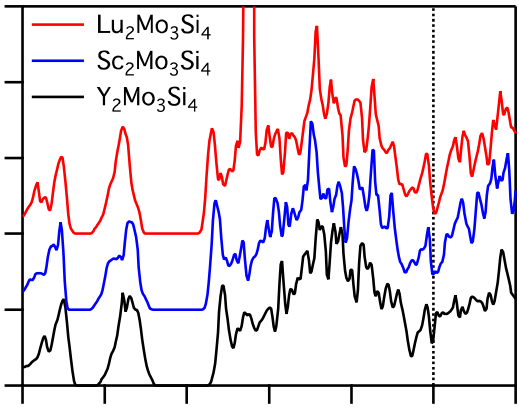

Figure 4. Total density of states of $Lu_2Mo_3Si_4$, $Sc_2Mo_3Si_4$ and $Y_2Mo_3Si_4$, offset from each other by 5 states/eV for clarity. The Fermi level rests at a pseudo-gap in all three compounds, with another such gap located about 2 electrons below, at -0.6 eV. Such a pseudo-gap is also present in Gd_5Si_4. The large peak in the Lu DOS is from the filled Lu *f* orbitals.

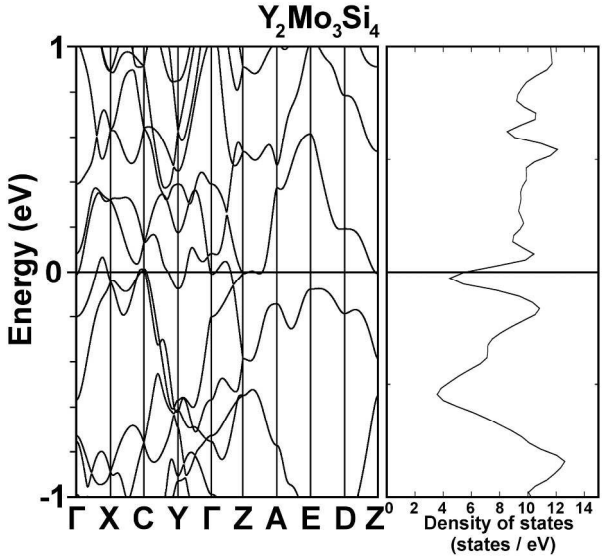

334

335 Figure 5. Electronic band structure of $P2_1/c$-symmetry $Y_2Mo_3Si_4$ and total density of states.

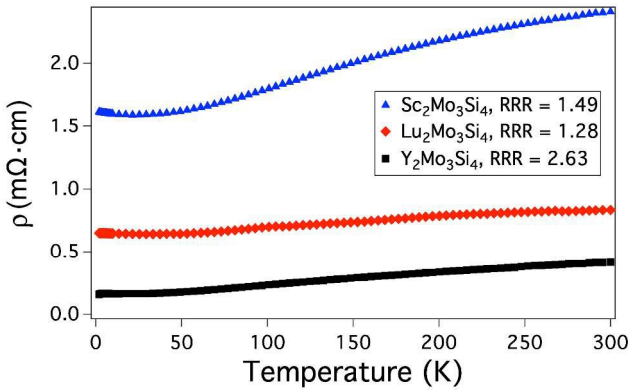

Figure 6. Resistivity of $Sc_2Mo_3Si_4$, $Lu_2Mo_3Si_4$ and $Y_2Mo_3Si_4$ as a function of temperature. The residual resistivity ratio (RRR = ρ(300K)/ρ(2K)) for each compound is also given, showing that they are all bad metals.

Table of Contents

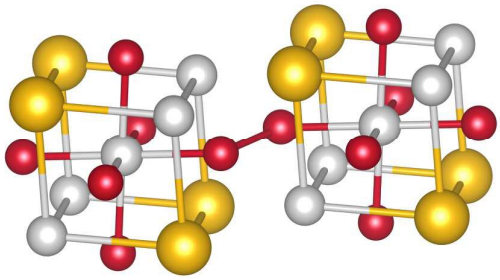

Four intermetallic silicides with Gd_5Si_4 structure were synthesized and characterized. Electronic and geometric factors govern cation order.